SSRG International Journal of Civil Engineering Volume 13 Issue 8, 137-151, August 2026
ISSN: 2348-8352/ https://doi.org/10.14445/23488352/IJCE-V13I8P108

Original Article

Effect of Void Depth on Flexural Strength, Ductility, and Strain Response of Hollow-Core RC Beams with Tension-Zone uPVC Conduits

Enow Ano Affuembey[1], Naftary GATHIMBA[2], John Nyiro Mwero[3]

[1]*Department of Civil Engineering, Pan African University Institute of Basic Sciences Technology and Innovation, Nairobi, Kenya.*
[2]*Department of Civil, Construction and Environmental Engineering, Jomo Kenyatta University of Agriculture and Technology, Nairobi, Kenya.*
[3]*Department of Civil and Resource Engineering, Technical University of Nairobi, Nairobi, Kenya.*

[1]*Corresponding Author : affuembey.enow@students.jkuat.ac.ke*

Received: 09 May 2026 Revised: 11 July 2026 Accepted: 09 August 2026 Published: 31 August 2026

Abstract *- Longitudinal voids formed by embedded conduits lessen the self-weight and material use of reinforced concrete beams. However, most publications regard the void as a passive cavity and ignore the contribution of the retained, bonded conduit. This paper investigates the relation of the void depth to the flexural response and ductility of hollow-core reinforced concrete beams with sand-coated unplasticized polyvinyl chloride conduits. The beams (150 × 250 × 1200 mm) were organized in five groups and subjected to a four-point bending test with a shear span-to-effective-depth ratio of a/d = 2.10. Pipe-in beams, which retained the sand-coated conduit at 0.29h and 0.42h from the soffit, and without pipe beams, which were voided at the same distances from the soffit, were also constructed. Pushout bond test provided a mean interfacial bond stress of 2.333 MPa, with a mean bond capacity of 14.66 kN, which exceeded the tensile capacity of the conduits, providing evidence that the sand-coated interfaces of the tested conduits achieved bond and fully tensioned the conduits before yielding of the conduits. The 0.29 h PI beam had the highest mean moment capacity at Mu = 26.197 kN·m (+11.85% over control). Pipe-wall strain gauges recorded* ε_{pvc} *= 0.01443 (above the uPVC yield strain of 0.01145). The 0.29 h WO beam had (μ = 10.74) and (Eabs = 2569.95 kN·mm) and achieved the highest ductility index and energy absorption while maintaining moment capacity within 3.03% of the control. The 0.42h PI beam had the lowest ductility (μ = 3.77) and energy absorption (975.80 kN·mm). ACI 318-19 nominal predictions underestimated absolute capacity across all groups but correctly reproduced the relative performance ranking. The findings indicate that void depth relative to the neutral axis, rather than void area alone, is the governing parameter in the load-ductility response of hollow-core RC beams with tension-zone uPVC conduits.*

Keywords *- Hollow-core RC beam, uPVC conduit, Void depth, Flexural ductility, Energy absorption, Composite bond.*

1. Introduction

The construction industry is still fighting to trim down embodied carbon and work with materials effectively. A popular method is to use less concrete. In a beam under positive bending, the section divides into an upper compression zone carried by concrete and a lower tension zone carried by steel, because concrete cracks at low tensile stress. After cracking, the concrete below the neutral axis contributes little to flexural strength while still adding self-weight [1, 2]. Casting a longitudinal void in this region therefore produces a lighter, more material-efficient member, and the same void can house electrical conduits, plumbing, or communication lines [3]. These benefits translate into lower dead load, reduced foundation demand, longer economical spans, and reduced natural-resource extraction and carbon emissions [4]. The structural response of a hollow-core beam differs from that of a solid beam because the void alters the internal stress field, the cracking pattern, and the failure mode. Earlier work on rectangular and square voids consistently reported reduced ultimate strength, lower stiffness, and larger deflection relative to solid controls, with the penalty growing as the void enlarged [5-7] Abbass et al. [8] studied flexible, high-strength beams and observed that with the size of the square opening (of size 60, 80, and 100 mm), the flexible, high-strength beam's deflection and strength were diminished, with the biggest size in the opening (100 mm) producing the greatest loss. Regarding circular voids, Elamary et al. [9] found that the loss of capacity was noticeable at approximately 10% of the beam's total cross-sectional area, and larger voids would cause a greater loss of capacity when the void area exceeds 10% of the beam area. Finally, for beams with circular and square voids, Manikandan et al. [10] found that beams with circular voids have a greater bending capacity than beams with square voids, perhaps due to less stress concentration with a circular boundary. Overall, the results of the previous studies show that a small-diameter circular void in the tension zone is justified.

The vertical location of a void is a second governing variable. Varghese and Joy [11] adjusted the depth of a circular hollow core and found the optimum core-center-to-depth ratio to be about 0.53. Sharaky et al. [12] employed a validated finite-element model to demonstrate that void location and dimension jointly characterize both the load capacity and the failure mode. Al-Maliki et al. [2] demonstrated that the placement of a void in the tension zone (rather than in the neutral axis) minimizes the reduction in flexural capacity. Murugesan and Narayanan [13, 14]analyzed the strength and deflection loss from a circular void and showed the loss was directly related to the void's location in the section. Alharthi et al. [15] and Abdulrahman [16] investigated hollow-core beams implemented with glass-fibre-reinforced-polymer (GFRP) bars, and Mansour et al. [17] placed aluminium sections into hollow self-compacting concrete beams. They all described how a stiff insert, which was glued to the surrounding concrete, regained some of the capacity the void had taken away. Furthermore, Du et al. [18, 19] and Yang et al. [20] increased the shear strength of damaged hollow-core members through cavity grouting and engineered-cementitious-composite jacketing. This collection of studies illustrates that the void former provides some bonding to the concrete and is capable of working as a load-sharing element instead of being a dead space. However, the case of a sand-coated uPVC conduit, which is a void former that is inexpensive and readily accessible, has not been explored, and bonding that would allow this composite action has been investigated in only a limited number of research studies.

Two gaps still exist. First, there has been no investigation of the combined impact of conduit depth and bond condition (retained and bonded versus removed) on the flexural strength, ductility, and strain within a single, controlled experimental study. Second, the retained uPVC conduit in bonded condition and the interfacial bond to the surrounding concrete have not been studied in the context of flexural testing. This research will address these gaps. Five beam groups were subjected to the same four-point bending tests, with the conduit positioned at two tension-zone depths (0.29h and 0.42h) and either retained as sand-coated permanent formwork or removed after the curing process. A supporting push-out test program established the bond between conduit and concrete. Pipe-wall strain gauges confirmed the composite action at the beam level. The primary focus of this research is to establish void depth as the primary variable, while articulating for the first time the bond-enabled composite contribution of the retained conduit and the opposing ductility of the system.

2. Materials and Methods

2.1. Beam Groups and Materials

Five RC beam groups (150 × 250 × 1200 mm) were cast: one solid control (BoF) and four hollow-core beams with Ø40 mm uPVC conduits. Each group had two nominally identical specimens (totaling ten beams). The presented data represent group averages, so the strength and ductility reflect replicated behavior rather than an individual specimen's variation. Conduits were positioned at 0.29h and 0.42h from the beam soffit to provide a comparison of a void that is deep in the tension zone (0.29h) relative to one that is closer to the neutral axis (0.42h), where the tension stress is lower. Conduits were either kept (pipe-in, PI) or cast as sand-coated permanent formwork or formed with a greased pipe that was extracted after curing (without-pipe, WO), as summarized in Table 1. The reinforcement and cross-sectional details of the three configurations are shown in Figure 1.

(a) **(b)** **(c)** **(d)**

(e)

Fig. 1 Cast beam specimens, (a) Sand-coated uPVC pipe with strain gauges attached, (b) Removable greased-coated wrapped uPVC pipe, (c) Sand-coated non-removable uPVC pipe, (d) Summary of beam cross-sections showing the solid control section and sections with and without a 40 mm conduit located at 0.29h and 0.42h from the bottom fibre, (e) Cured beams after 28 days.

Three justifications were made for the selection of the Ø40 mm conduit diameter. First, the conduit diameter matches the most commonly used electrical and service conduit sizes in regional practice. Second, the void area of the cross-section of the selected conduit diameters remains at about 3.4%, much lower than the ~10% threshold above which a remarkable reduction of the load-bearing capacity occurs. Third, the selected diameter preserved a clear cover to the tension steel so that the bar bond was not disturbed. Based on section analysis, two of the selected conduit sizes were chosen based on bracketing the tension zone, as opposed to providing an extensive sample, thereby offering a controlled contrast of a deep and shallow tension-zone void.

Table 1. Experimental beam group details

Beam Group ID	Description	Configuration	Ø40 uPVC Pipe position (h)
BoF	Control	Solid beam	Reference
Flex 1	Pipe in	Sand-coated pipe	0.29h
Flex 2	Pipe in	Sand-coated pipe	0.42h
Flex 3	No pipe in	Removed greased uPVC	0.29h
Flex 4	No pipe in	Removed greased uPVC	0.42h

The cement used for concrete was OPC 42.5 CEM II, with river sand having a fineness modulus of 2.61, and coarse aggregate of crushed granite with a nominal size of 20 mm, along with a water-cement ratio of 0.45 and a mix proportion of 1:1.54:2.72. To avoid segregation and honeycombing at the surface of the conduit and thus weakening the matrix bond, the maximum size of coarse aggregate was limited to 20 mm. The hardened concrete developed a cube compressive strength of 30.52 MPa and a 28-day split tensile strength of 2.70 MPa as shown in Table 2. The concrete section was reinforced with two tension bars of 10 mm diameter (fy = 460 MPa, Es = 200 GPa, As = 157.1 mm^2) and two compression bars of 8 mm diameter and 8 mm diameter stirrups with 100 mm spacing. The mechanical properties of the uPVC conduit obtained from tension coupon tests showed Apvc = 250 mm^2, fpvc = 34.34 MPa, Epvc = 3000 MPa, εy_{pvc} = 0.01145, and a tensile capacity of Tpvc = 8.585 kN. Section analysis to ACI 318-19 [21] showed a Whitney compression-block depth of a = 23.2 mm and indicated a tension-controlled section. Also, both voids (72.5 mm at 0.29 h and 105 mm at 0.42 h from the soffit) are fully within the tension zone.

Table 2. Aggregate and concrete characterization results

Test	Result	Limit / Req.
Fine Agg. Specific Gravity (Gs)	2.63	2.50-2.70
Coarse Agg. Sp. Gr. SSD (Gs)	2.55	2.50-2.75
Fine Agg. Fineness Modulus	2.61	2.3-3.1
Coarse Agg. Max. Size	20 mm	≤ 25 mm
Agg. Impact Value (AIV)	6.2%	< 30 %
Agg. Crushing Value (ACV)	20.2 %	< 25 %
Cube Comp. Strength. (28d)	30.52 MPa	≥ 25 MPa (C30)
Tensile Strength of Cylindrical Concrete. (28d)	2.70 MPa	-

The aggregate met all of the structural requirements. The AIV of 6.2% and ACV of 20.2%, both fall within the limits for structural concrete. The graded properties also fulfilled the requirements of BS EN 933-1 [22] and BS 812 [23] Split tensile strength was determined as outlined in the ASTM C496/C496M-17 [24].

2.2. Push-Out Test

Four push-out specimens, SP1 to SP4, quantified the interfacial bond of the sand-coated conduit. The setup contained a 150 mm by 100 mm concrete block with a centrally located uPVC conduit (40 mm in diameter) bonded over 50 mm of the sand-coated length with Sikadur-31 CF epoxy (tensile modulus of 3000 MPa, tensile strength of 27 MPa). Loading was set at a rate of 0.5 kN/min. Slip was measured using two LVDTs. This configuration is shown in Figure 2. The mean bond stress was calculated as shown in Table 3.

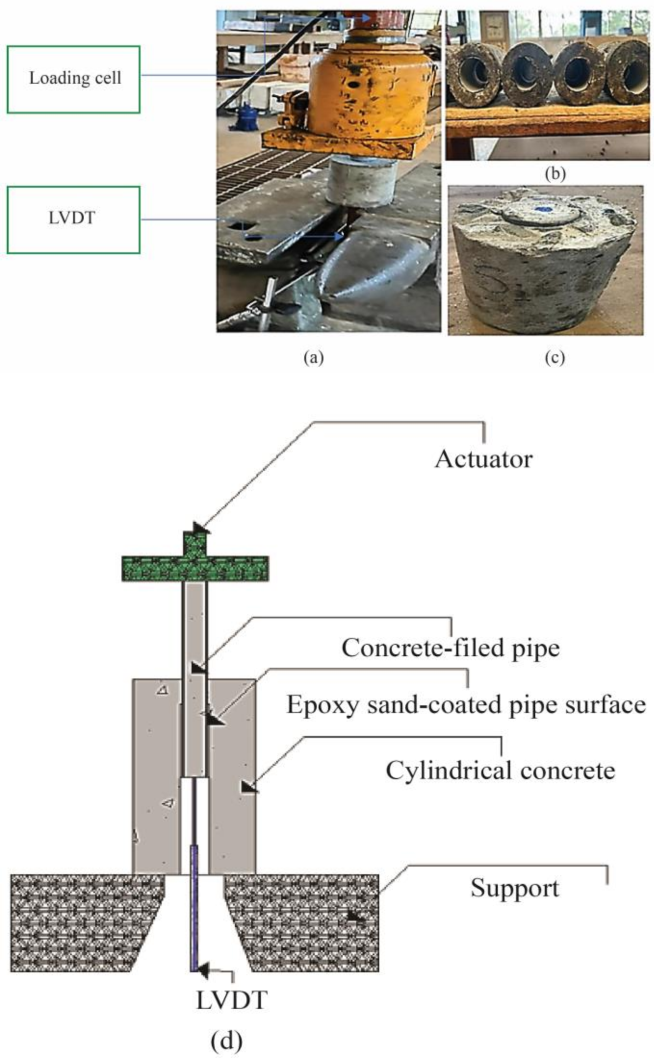

Fig. 2 Shows the setup of the laboratory test for the pushout bond test, (a) Shows the mounted pushout cylinder, (b) Shows the push-out part, (c) Shows the pushed-out sample, and (d) Shows a schematic pushout representation.

$$\tau = \frac{P}{\pi DL} \qquad (1)$$

Where P is the applied load, D is the outer diameter of the conduit, and L is the bonded length, assuming a uniform stress distribution on the contact area, which is πDL [25].

Table 3. Push-Out bond test results (SP1- SP4)

Group Spe ID	Mean Peak Load (kN)	Mean Slip at Peak (mm)	Mean Bond Stress (MPa)	Energy Abs. (kN·mm)
SP1	14.292	0.540	2.275	1.679
SP2	14.689	0.560	2.338	2.062
SP3	14.554	0.530	2.316	1.649
SP4	15.086	0.553	2.401	2.009
Mean	14.655	0.546	2.333	1.850

The bond stress coefficient of variation across specimens was just 2.3%, an indicator of a reliable interface. The average bond capacity was 14.66 kN compared to a conduit tensile capacity of 8.59 kN. The bond capacity was 1.71 times the tensile capacity. This shows that the sand-coated interface is capable of developing the full conduit tension before slip occurs. This difference is the mechanical justification for considering the retained conduit as a composite tensile component of the pipe-in beams. The typical load-slip behavior for the four specimens is shown in Figure 3.

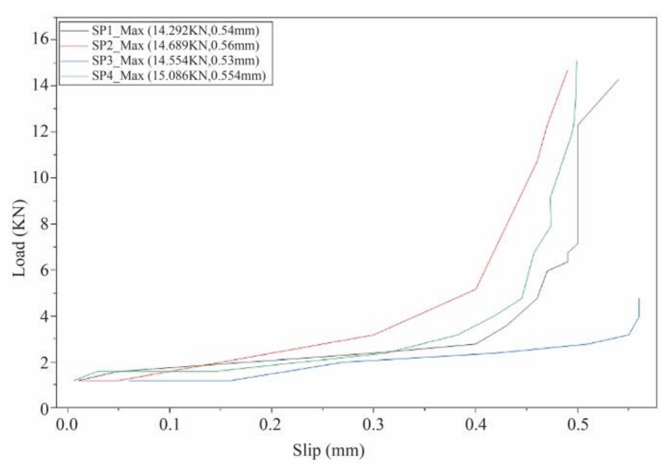

Fig. 3 Representative load-slip response of the four push-out specimens (SP1-SP4)

2.3. Flexure Test Protocol

Four-point bending was conducted with a clear span of 1000 mm and a shear span-to-effective-depth ratio of a/d = 2.10, with each shear span measuring 450 mm, and loading was applied in the mid-span. LVDT was used to measure the mid-span deflection. Before the test, strain gauges were installed on the top and bottom concrete fibres, and on the top and bottom fibres of the steel section, and on the side steel, for the pipe-in-beams, strain gauges were attached at the mid-span of the constant-moment zone of the outer bottom wall of the conduit. During the test, loading was conducted under a controlled load of 0.5 kN/min until either failure or an 80% decrease from the peak load occurred. The first crack for each test was documented and was the point of a kink in the load-deflection plot. The four-point bending setup is illustrated in Figure 4.

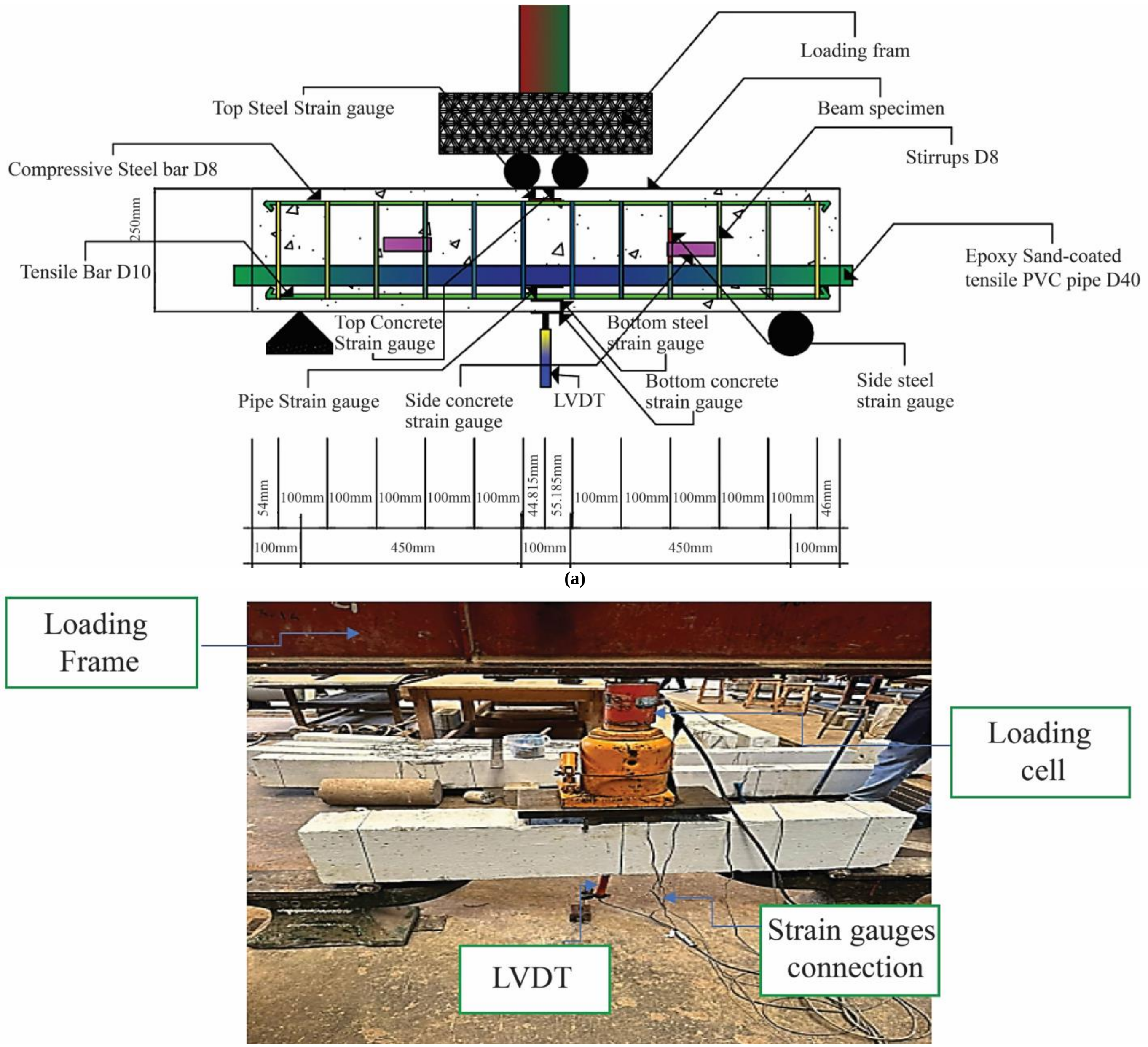

Fig. 4 Four-point bending test set-up, (a) Schematic of the loading arrangement with dimensions, (b) photograph of a beam in position on the testing machine before loading.

3. Results and Discussion

3.1. Load-Deflection Response

The averaged load-deflection curves of all five groups reveal four phases. The first is an elastic branch of pre-cracking that stops at the cracking load Pcr (30.5 - 35.25 kN). The second phase is a post-cracking branch with reduced stiffness. In this phase, the stiffness of PI beams was greater than that of WO beams due to composite conduit action. This was followed by a nearly yield transition and a descending post-peak branch. In the post-cracking section, PI and WO curves exhibit a clear difference. This difference is the result of the bonded conduit that is exerting tension through the crack. Mean load-deflection curves are illustrated in Figure 5.

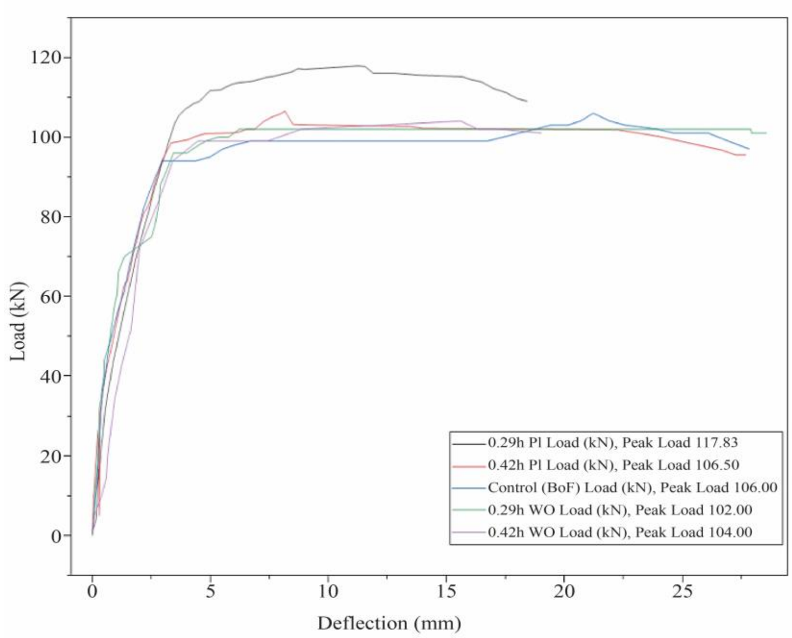

(a)

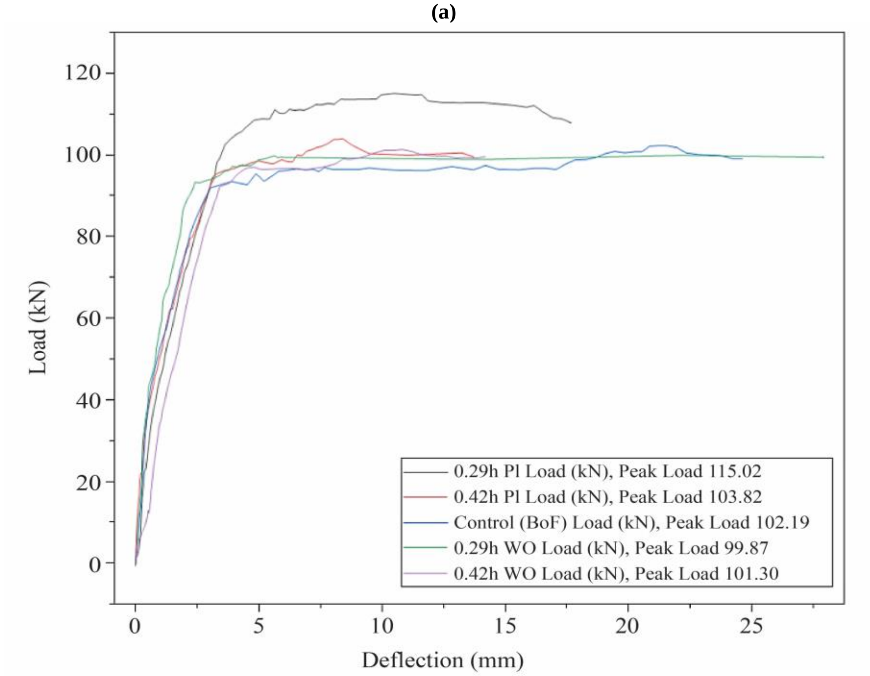

(b)

Fig. 5 Load-mid-span deflection curves for the five flexural beam groups

3.2. Ultimate Moment Capacity

The ultimate moment was obtained from the four-point bending relation

$$M_u = \frac{P_u\, a}{2} \quad (2)$$

where Pu represents the ultimate load and a is the shear span. Here, the yield load was taken as Py = 0.75 Pu based on the bilinear Park criterion [26], which describes the behavior of the present beams because the PI specimens exhibit a smeared post-cracking phenomenon with no distinctly sharp yield plateau. Because both voids are located completely within the tension zone and do not affect the compression block, the WO capacities stayed close to the control. The PI beams develop strength through composite conduit tension. At 0.29h, the conduit is fully yielded (ε_{pvc} = 0.01443 > εy_{pvc} = 0.01145; T_{pvc} = 8.585 kN). At 0.42h, the conduit is not fully yielded and contributes a limited amount of strength ($\varepsilon_{pvc} \approx$ 0.01126).

3.3. Performance Metrics - Full Results Table

Table 4. Averaged experimental flexural performance matrix

Group Average	Pu (kN)	Py (kN)	Mu (kN·m)	ΔMu vs Control	δy (mm)	δu (mm)	μ = δu/δy	Eabs (kN·mm)	Pcr (kN)
Control (BoF)	104.1	78.07	23.422	Ref	2.24	21.19	9.49	2115.55	35.25
0.29h PI	116.43	87.32	26.197	+11.84%	2.72	10.88	4.01	1579.75	32.59
0.42h PI	105.16	78.87	23.661	+1.02%	2.15	8.11	3.78	975.8	34.01
0.29h WO	100.94	75.67	22.712	-3.04%	2.4	25.77	10.74	2569.95	30.5
0.42h WO	102.65	76.99	23.096	-1.39%	1.84	13.22	7.14	1295.7	32.82

Where Pu = ultimate load; Py = yield load; Mu = ultimate moment; δy, δu = yield and ultimate deflection; μ = displacement ductility index; Eabs = absorbed energy to peak load (trapezoidal rule); Pcr = cracking load. Ductility values follow the classification framework of Asiani et al. [27]. These results fall within the range of variation for laboratory RC flexural tests. Pairwise comparison of the means indicated that the 0.29h PI group (116.43 kN) was significantly different from the control (104.10 kN) and that the observed +11.85% strength gain was not due to variability of the specimens. In contrast, the other voided groups besides the 0.29h PI group overlap the control group in ultimate load due to the tension zone voids leaving the compression block unchanged.

3.4. Discussion of Strength and Ductility

The 0.29h PI beam reached the highest moment capacity via full composite conduit yield (+11.85%). This was confirmed by the pipe-wall gauges. The yield of the conduit resulted in a significant loss of ductility (μ = 4.00). Conduit yield causes loss of stable post-yield reserves in the section and causes a localized stiffening around the bonded former.

The 0.42h PI beam had a near-but-below-yield conduit, which was also nearly the same as the control beam (+1.02%). This beam had the lowest ductility (μ = 3.77), which was due to the placement of the conduit near the neutral axis.

The stiff conduit disrupts the compressive resistance path at large deflection without contributing meaningful tension, giving the worst strength-to-ductility outcome. The moment-capacity comparison and the ductility results are shown in Figure 6 and Figure 7, respectively.

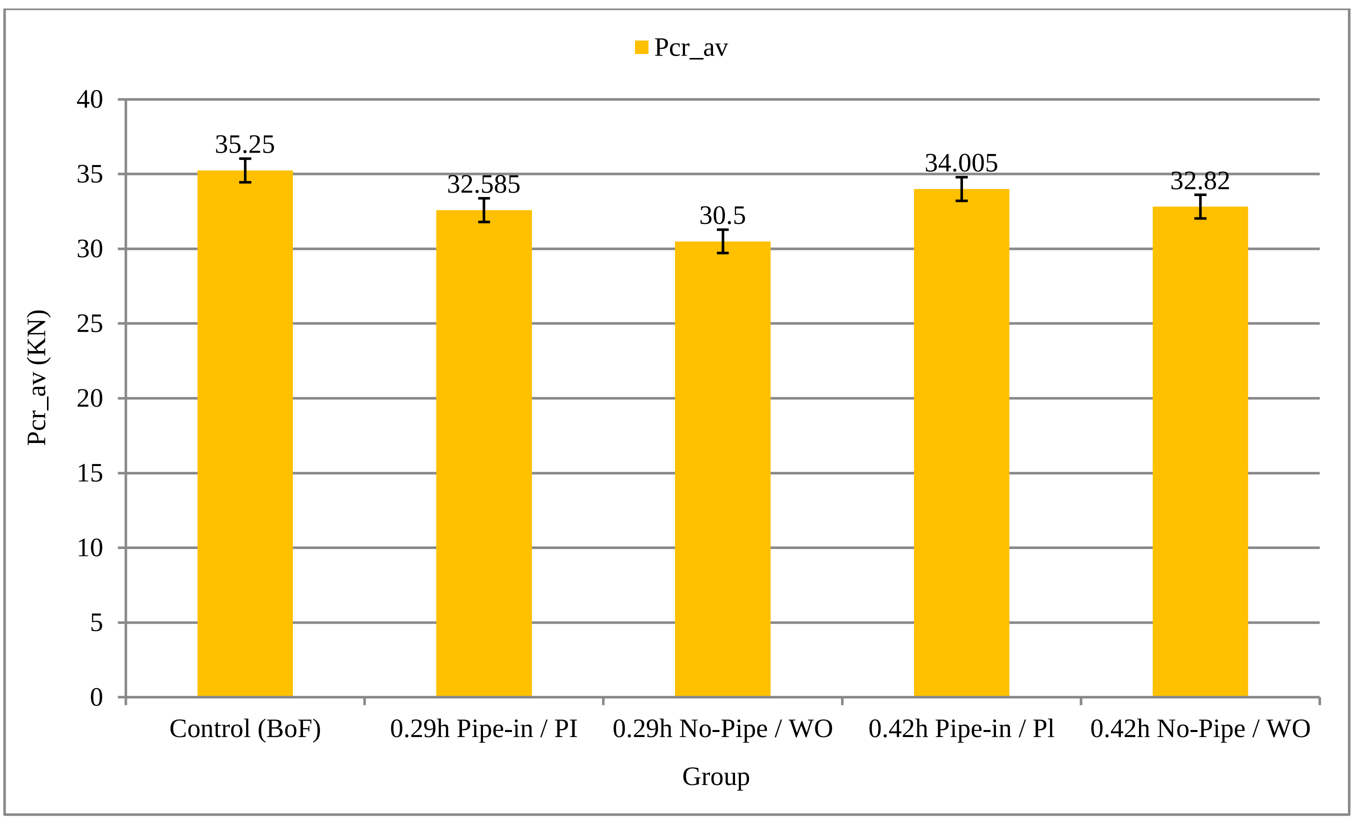

Fig. 6 Ultimate moment capacity of the five beam groups relative to the control

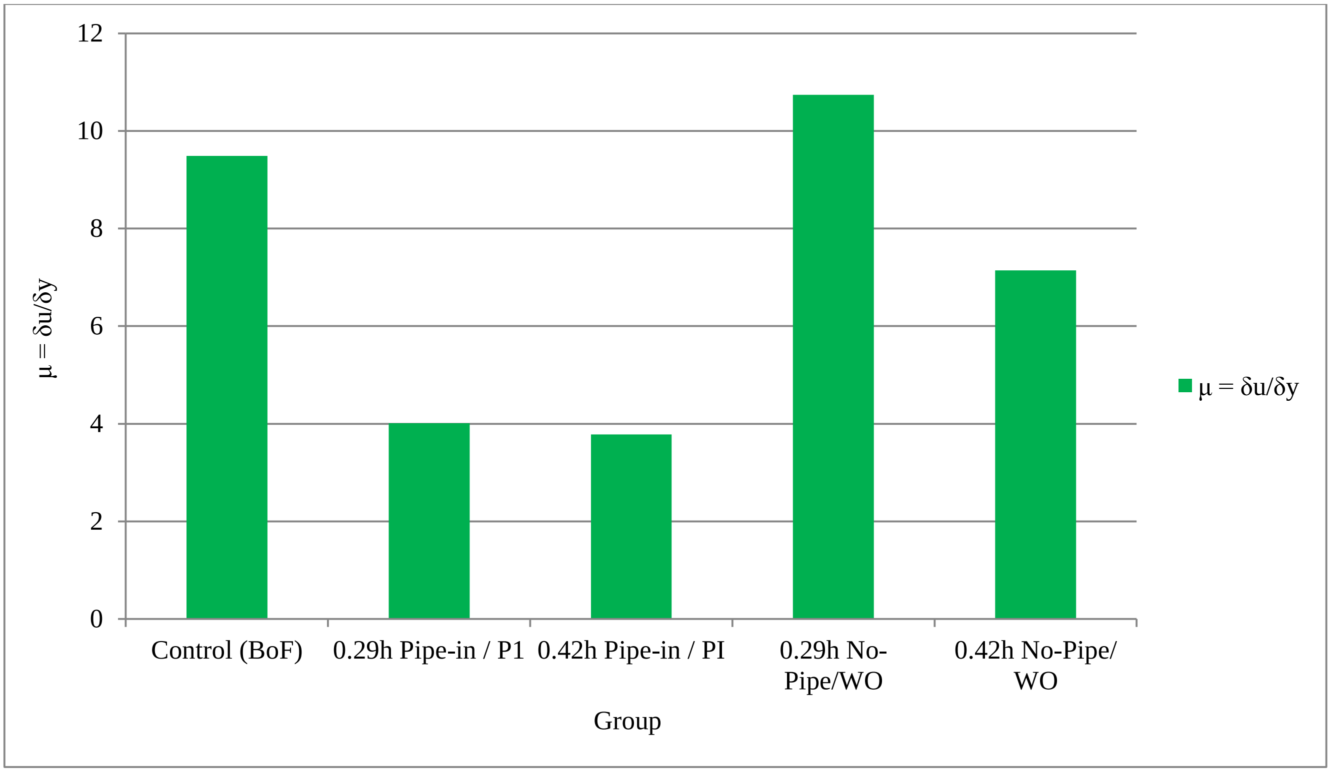

Fig. 7 Displacement ductility index by beam group

For both WO groups, moment capacity was within 3.1% of the control. This shows that a tension-zone void that does not intersect with the compression block hardly impacts the strength. The 0.29h WO beam had the best balance, having the highest ductility ($\mu = 10.74$) and the highest energy absorption ($E_{abs} = 2569.95$ kN·mm, +21.5% control) while also keeping moment capacity within 3.03% of the control. With the removal of cracked tension-zone concrete with low contribution and the retention of the full compression flange, the section can deflect more before ultimate failure. The 0.42h WO beam was mid-range ($\mu = 7.18$; $E_{abs} = 1295.70$ kN·mm) since voids, at a distance of 105 mm from the soffit, approach the neutral axis at large deflection and promote earlier concrete splitting.

The cracking loads (30.5 - 35.25 kN) exhibited a consistent hierarchy, with the solid control cracked last and the 0.29h WO beam cracked first; the PI beams cracked at intermediate loads because the tension across the forming crack was partially carried by the bonded conduit wall. This hierarchy was maintained in the replicate specimens.

3.5. Comparison with the State of the Art

The current results add to existing literature and show some similarities. The existing literature on open square and rectangular voids shows net strength reductions of 10 - 30% [5, 6, 8]. In contrast to those results, WO beams lost net strength by only 3.1%. This was attributed to the void size (~3.4% of the cross-section) and location (in the tension zone) of the circular voids, which was very close to the sub-10% limit proposed by Elamary et al. [9]. The earlier reinforced-insert research used GFRP bars [15, 16] and aluminum sections [17] to restore the lost capacity. The current research shows a greater net strength increase (+11.85%) of sand-coated uPVC conduit and, most importantly, explains the strength increase based on directly measured bond strength and not assumed bond strength. The results also show that the same sand-coated uPVC conduit inserts that explain increased strength at 0.29h also reduce the ductility of the system. Considering that flexibility and strength explain the result for retained plastic conduits, the results also indicate that the same uPVC conduit inserts that increase system strength also reduce ductility.

3.6. Strain Response

The peak load compressive strains of top-fibre concrete for WO and the control beams showed values of -1800 με and -2600 με, respectively, which are all ACI 318-19 crushing strain of -3000 με. Therefore, all the beams failed in flexural tension due to steel yielding and not due to concrete crushing. The position of the neutral axis at ultimate for the WO and control beams was about 27 mm (12.8% of d = 214 mm), and for the PI beams it was about 31 mm (14.3% of d). The deeper neutral axis of the PI beams indicates the additional tension contributed by the bonded conduit. The resulting neutral axis positions place the sections in the tension-controlled regime. The average load-strain responses of each group are shown in Figure 8.

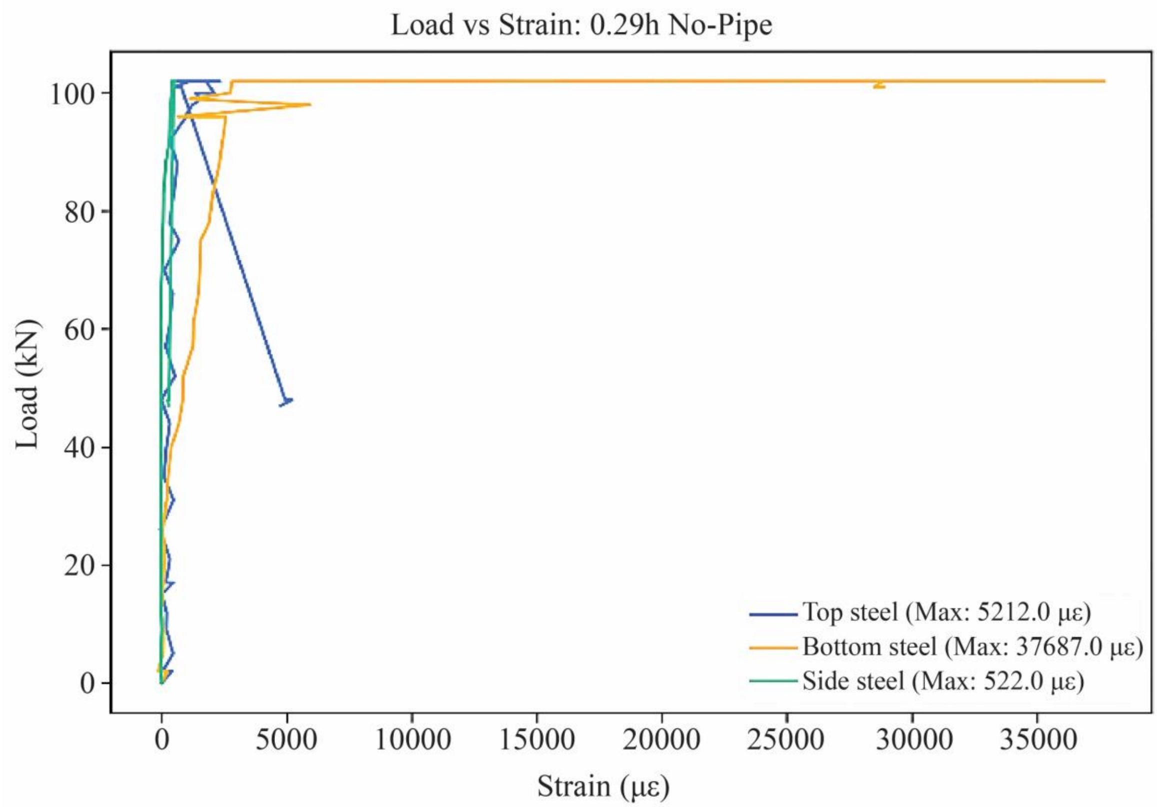
Load vs Strain: 0.29h No-Pipe
Load (kN)
Strain (με)
Top steel (Max: 5212.0 με)
Bottom steel (Max: 37687.0 με)
Side steel (Max: 522.0 με)
0
20
40
60
80
100
5000
10000
15000
20000
25000
30000
35000

(a)

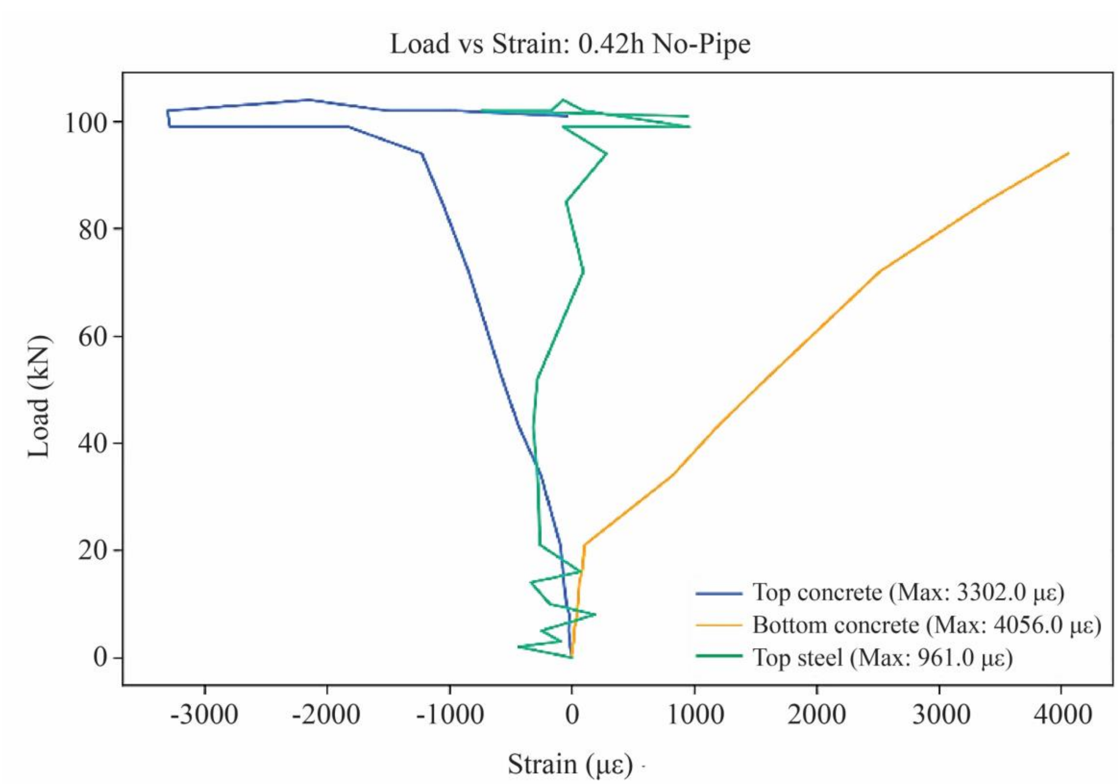
Load vs Strain: 0.42h No-Pipe
Load (kN)
Strain (με)
Top concrete (Max: 3302.0 με)
Bottom concrete (Max: 4056.0 με)
Top steel (Max: 961.0 με)
-3000
-2000
-1000
0
1000
2000
3000
4000
20
40
60
80
100

(b)

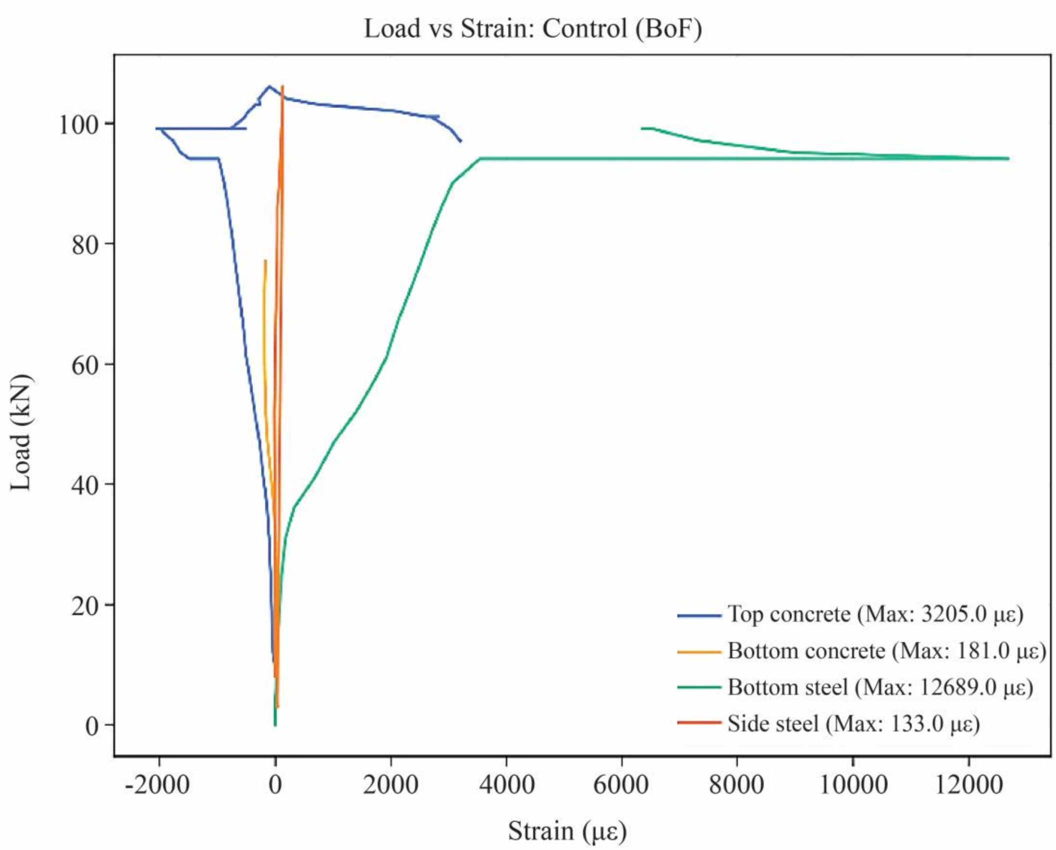
Load vs Strain: Control (BoF)
Load (kN)
Strain (με)
0
20
40
60
80
100
-2000
0
2000
4000
6000
8000
10000
12000
Top concrete (Max: 3205.0 με)
Bottom concrete (Max: 181.0 με)
Bottom steel (Max: 12689.0 με)
Side steel (Max: 133.0 με)

(c)

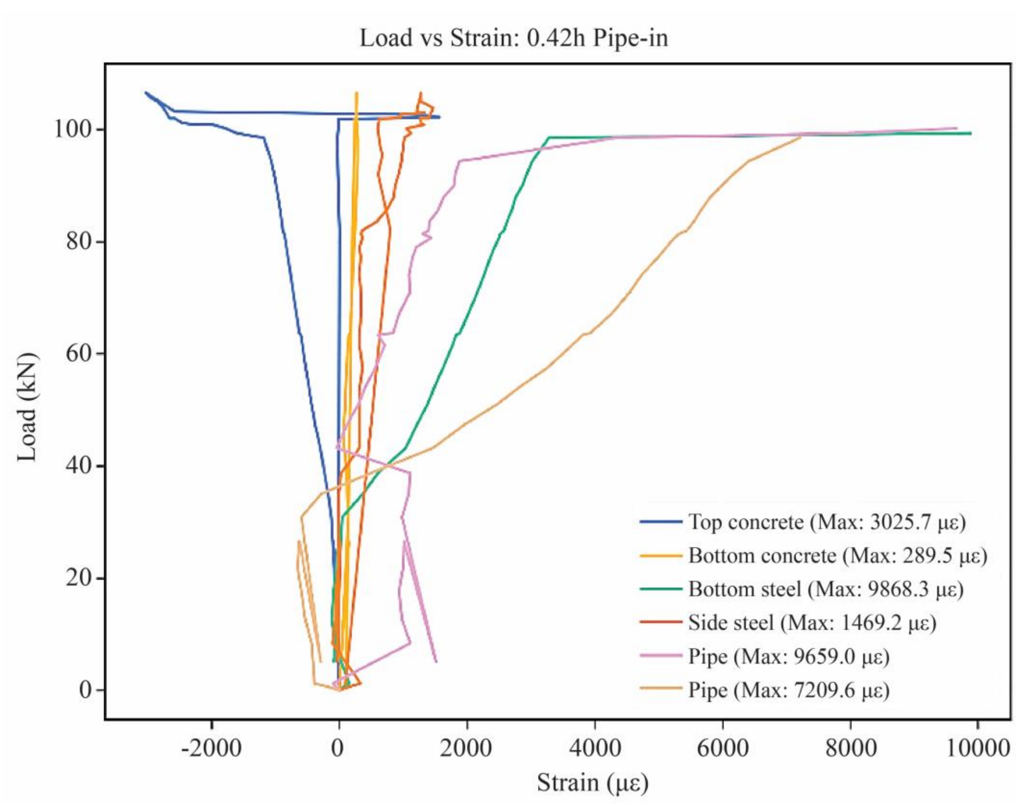
Load vs Strain: 0.42h Pipe-in
Load (kN)
Strain (με)
0
20
40
60
80
100
-2000
0
2000
4000
6000
8000
10000
Top concrete (Max: 3025.7 με)
Bottom concrete (Max: 289.5 με)
Bottom steel (Max: 9868.3 με)
Side steel (Max: 1469.2 με)
Pipe (Max: 9659.0 με)
Pipe (Max: 7209.6 με)

(d)

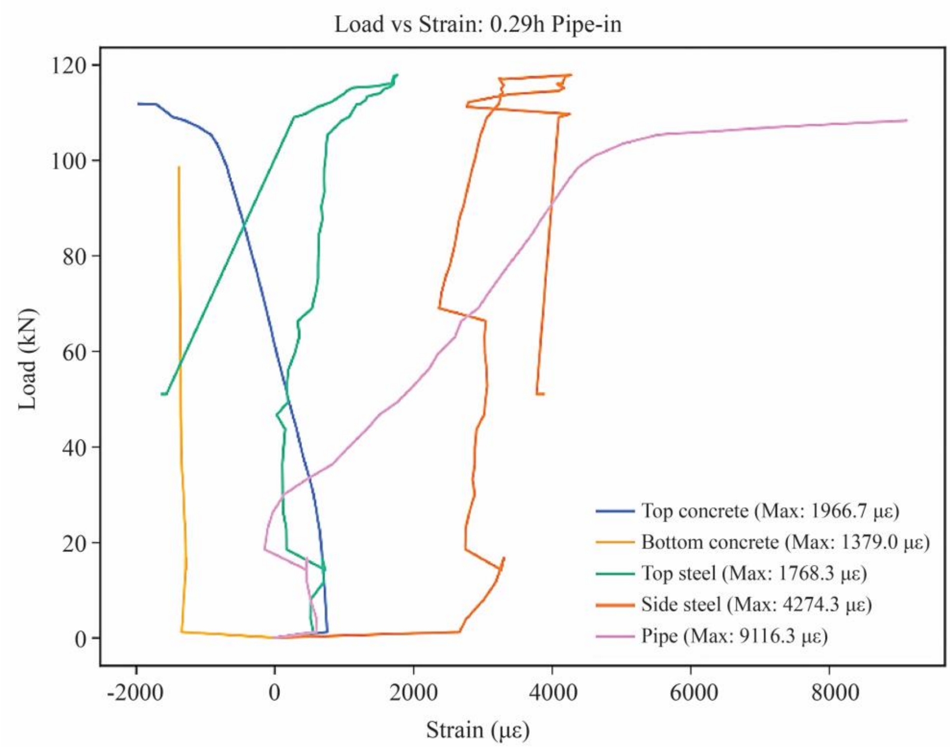

(e)

Fig. 8 (a) to (e) Represent the mean Load vs. Strain (με) per beam group, Pipe-wall gauges confirm composite tensile participation, WO beams accumulate strain 25 - 40% faster, indicating accelerated post-crack stiffness loss.

The pipe-wall gauges measured mean strain ranges at 0.29 h and 0.42 h as 350-9116 and 200 - 8434 με, respectively. This indicates participation of composite tensile members and suggests that at the beam scale, the epoxy bond (τ = 2.333 MPa) was able to sustain strain compatibility. The WO beams exhibited strain accumulation per unit deflection at a rate 25 - 40% higher than the PI and control beams. This is a quantitative serviceability indicator of the accelerated loss of post-crack stiffness in the absence of tensile members and without replacement of the tensioning conduit.

3.7. Crack Pattern and Failure Mode

Table 5 shows the cracked-section secant stiffness K between cracking and yield. The PI beams at both depths are stiffer than the WO beams. This shows that bonded conduit does provide some measurable tension stiffening. This means that close to the neutral axis, the stiffening contribution of the conduit can counter the stiffness lost to the void. This is because at the neutral axis, the lost flexural lever arm is less important.

Table 5. Cracked-Section secant stiffness

Group	0.75Pu (kN)	0.75Pu - Pcr (kN)	δy - δcr (mm)	K (kN/mm)
Control	78.07	42.82	1.81	23.7
0.29h PI	87.32	54.73	2.17	25.2
0.42h PI	78.87	44.86	1.73	25.9
0.29h WO	75.70	45.20	2.12	21.3
0.42h WO	76.99	44.17	2.30	19.2

3.8. Failure Behaviour and Crack Propagation

All beams exhibited only flexural tension failure. There was no shear failure or concrete crushing. The top-fibre strains remained (-1800 to -2600 με) and were below the crushing limit. The first vertical cracks appeared at the soffit in the load range of 30.59 - 34.01 kN. These cracks extended towards the neutral axis with increasing load. Control and WO beams had similar ranges of number of well-distributed flexural cracks with ductile behavior (μ = 7.18 - 10.74). PI beams had a large number of smaller, well-distributed cracks due to the bonded conduit that transferred the tension across beams and went brittle afterwards when the conduit failed. The 0.42h PI beam was the most brittle (μ = 3.77) and had the lowest energy absorption (975.80 kN·mm). This provides additional evidence that the failure mode, similar to strength and ductility, is dependent on the depth of the void relative to the neutral axis and whether the conduit is bonded or not. The failure modes and observed crack pattern are shown below in Figure 9.

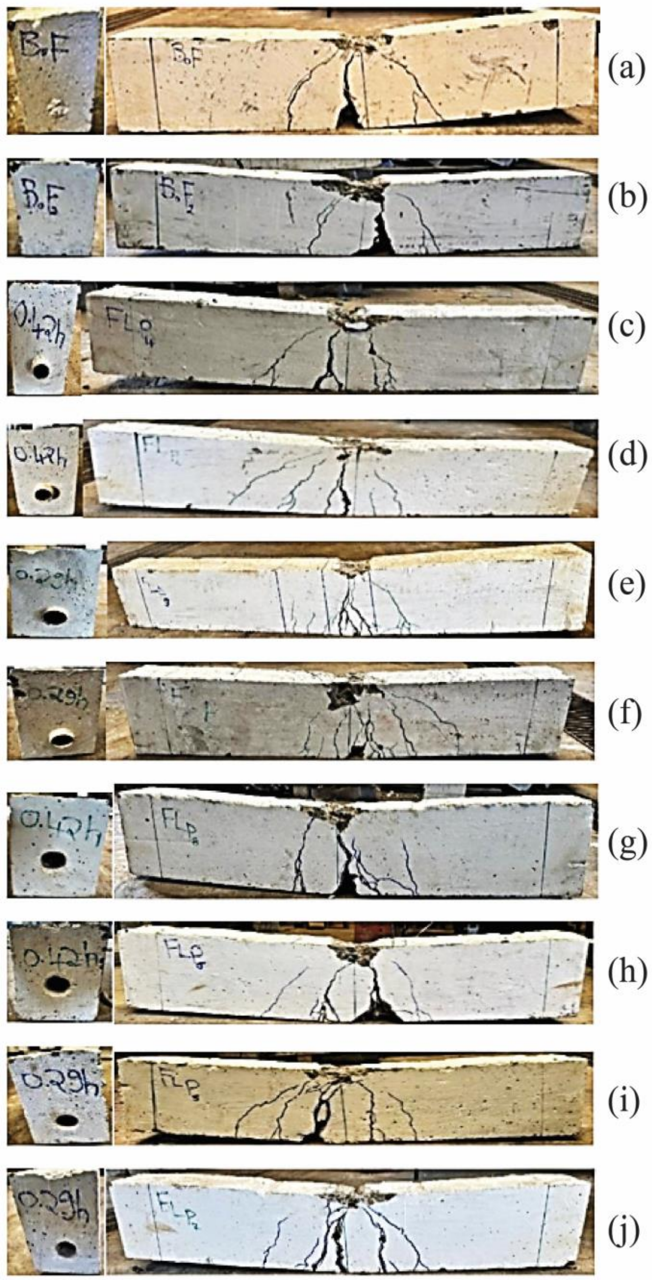

Fig. 9 Failure modes of all tested beams (a) to (e) for group 1 and (f) to (j) for group 2, for Control beam, PI and WO beams.

3.9. Theoretical Analysis and Comparison with ACI 318-19.

Closed-form predictions in ACI 318-19 were used to validate experimental capacities as represented in Figure 10. The material properties for the experiment were derived from the cube strength measurements (fc_{cube} = 30.52 MPa):

$$f'_c = 0.80\, f_{c,cube} = 24.42 \text{ MPa} \quad (3)$$

$$E_c = 4700\sqrt{f'_c} = 23{,}224 \text{ MPa} \quad (4)$$

$$f_r = 0.62\sqrt{f'_c} = 3.064 \text{ MPa} \quad (5)$$

$$\beta_1 = 0.85 \quad (f'_c \leq 28 \text{ MPa}) \quad (6)$$

Nominal Flexural Capacity (β1 = 0.85), the stress-block depth and moment capacity for the control and WO beams are:

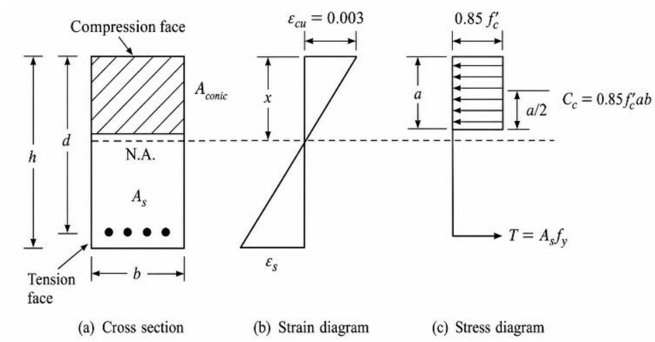

Fig. 10 Whitney rectangular stress block

For the control and WO beams, the Whitney rectangular stress block [28] gives

$$a = \frac{A_s f_y}{0.85 f'_c b} = \frac{157.1 \times 460}{0.85 \times 24.42 \times 150} = 23.2 \text{ mm} \quad (7)$$

$$M_n = A_s f_y \left(d - \frac{a}{2}\right) = 14.62 \text{ kN·m} \quad (8)$$

For the PI beams, the bonded conduit provided a tensile force $T_{pvc} = A_{pvc}\, f_{pvc}$ = 250 × 34.34 = 8585 N, so the block depth and moment become

$$a_{PI} = \frac{A_s f_y + T_{pvc}}{0.85 f'_c b} \quad (9)$$

$$M_{n,PI} = A_s f_y \left(d - \frac{a_{PI}}{2}\right) + T_{pvc}\left(y_{pvc} - \frac{a_{PI}}{2}\right) \quad (10)$$

Where y_{pvc} is the depth of the conduit centroid below the top fibre. For the pipe-in beams, this yields a value of a_{PI} = 25.97 mm and the design moment for the pipe-in sections is given as Mn_{PI} = 15.94 kN·m (0.29h) and 15.66 kN·m (0.42h).

The predicted capacities for all beam groups were lower than the measured capacities, and the predicted over-strength ratio was in the range of 1.51 - 1.64 (1.60 for the control beams, 1.55 - 1.58 for the WO beams, and for the PI-beams, 1.64 and 1.51 for the 0.29h and 0.42h sections, respectively, based on the composite nominal moments). The difference in predicted and actual capacities is attributed to the time-dependent increase in concrete strength after 28 days, post-yield strain hardening of the steel ($f_u \approx 1.28\ f_y$ = 588.8 MPa), and the additional tension for the PI beams, due to the bonded conduit. Even with the underprediction of capacities, the correct rank order of the beam groups was predicted.

$$M_{u,0.29h\,PI} > M_{u,0.42h\,PI} > M_{u,Control} > M_{u,0.42h\,WO} > M_{u,0.29h\,WO}$$

All sections were confirmed to be tension controlled (εs = 0.018 - 0.021, much greater than ε_y = 0.0023). Additionally, top-fibre strains ended up being less than -3000 $\mu\varepsilon$, which is the crushing limit.

This model is reliable for ranking and doing the first pass of sizing for the configurations and parameters; however, a calibration factor of approximately 1.5 - 1.65 is still required to achieve the correct capacity.

3.10. Practical Considerations

Numerous other factors influence field usage apart from the mechanical outcomes. Constructability: the sand-coated conduit can function as permanent internal formwork; therefore, no void former needs to be withdrawn. The greased-removal (WO) route requires a delicate removal procedure and is better suited for precast conditions because it disturbs the green concrete.

Durability of the uPVC: uPVC exhibits good moisture and chemical resistance; however, the PI configuration and its structural integrity rely on the bond of the epoxy, and thus the effect of early aging on the epoxy under the conditions of prolonged subjection to a combination of moisture and atmospheric temperature and pressure should be studied before any field application.

Fire and serviceability: uPVC softens at moderate temperatures; therefore, in members that will be exposed to fire the contribution of the conduit to the overall member's tension should be considered as a serviceability rather than ultimate reserve, and sufficient concrete cover should be maintained; under service loads, the PI beams' tension stiffening should be considered as a beneficial deflection control. These will constitute the results of the present tests in aid of design and will define the limits of what the current monotonic tests can cover.

4. Conclusion

The five RC beam groups subjected to four-point bending (a/d = 2.10) and supported by push-out bond characterization and strain gauging led to the following conclusions.

1. Retaining the sand-coated uPVC conduit (located at 0.29h) and leading to composite PVC tensile action (ε_{pvc} = 0.01443 > $\varepsilon_{y,pvc}$ = 0.01145) at the expense of reduced ductility (μ = 4.00) and energy absorption relative to the control, the mean moment capacity increased by 11.85%.
2. The 0.29h beam without the pipe, which achieved the highest ductility (μ = 10.74) and energy absorption (2569.95 kN·mm), achieved the best strength–ductility balance and maintained the moment capacity within 3.03% of the control.
3. The 0.42h pipe-in configuration, which led to a minor strength increase of +1.02%, was the least favorable for deformation and showed the lowest ductility (μ = 3.77) and energy absorption (975.80 kN·mm) due to inefficiency from the conduit being aligned at the neutral axis.
4. Both beam configurations without the pipe maintained moment capacity within 3.1% of the control, and demonstrated that a tension-zone void of a small size that does not intersect the compression block does not significantly affect the flexural strength.
5. From the push-out bond tests, the average bond stress was 2.333 MPa, with bond capacity (14.66 kN) exceeding the conduit tensile capacity by 1.71 times, supporting the mechanical explanation of composite action in the pipe-in beam cases.
6. ACI 318-19 showed some underestimation of the actual capacity (Ω = 1.51 - 1.64), but the correct order was predicted, meaning, for a preliminary design, the nominal equation can be used in combination with a calibration factor.

Overall, the depth of the void in relation to the neutral axis (rather than simply the void area) impacts the strength and ductility of tension-zone hollow-core RC beams (with uPVC conduits).

Further research should investigate a larger depth range of 0.29h - 0.42h and include other conduit diameters and concrete quality; incorporate cyclic and seismic loading to evaluate the behavior of bonded conduit with low flexural ductility during loading reversals; and perform aging simulations to study the bonded conduit-to-concrete interface under prolonged conditions of load, humidity, and temperature before establishing the pipe-in-tube configuration for service.

Conflict of Interest

The authors declare no conflict of interest.

Data Availability

Data supporting this article can be obtained from the corresponding author by request.

Funding Statement

The African Union, funded through the Pan-African University Institute of Basic Sciences, Technology and Innovation, supported this work.

Acknowledgments

The authors acknowledge support from the African Union for funding and from the Department of Civil Engineering at the Pan-African University (PAUSTI) and the Jomo Kenyatta University of Agriculture and Technology (JKUAT) for the provision of laboratory facilities and technical support.

References

[1] David Darwin, Charles William Dolan, and Arthur H. Nilson, *Design of Concrete Structures*, Fifteenth Edition, McGraw-Hill Education, pp. 1-786, 2016. [Google Scholar] [Publisher Link]

[2] Hadi Naser Ghadhban Al-Maliki et al., “Structural Efficiency of Hollow Reinforced Concrete Beams Subjected to Partial Uniformly Distributed Loading,” *Buildings*, vol. 11, no. 9, pp. 1-16, 2021. [CrossRef] [Google Scholar] [Publisher Link]

[3] Ali Said Alnuaimi, Khalifa S. Al-Jabri, and Abdelwahid Hago, “Comparison between Solid and Hollow Reinforced Concrete Beams,” *Materials and Structures*, vol. 41, no. 2, pp. 269-286, 2007. [CrossRef] [Google Scholar] [Publisher Link]

[4] Haider M. Abdulhusain, and Murtada A. Ismael, “Structural Behavior of Hollow Reinforced Concrete Beams: A Review,” *Diyala Journal of Engineering Sciences*, vol. 13, no. 4, pp. 91-101, 2020. [CrossRef] [Google Scholar] [Publisher Link]

[5] R. Othman et al., “Experimental Study on Flexural Behaviour of Reinforced Foamed Concrete Square Hollow Beam,” *IOP Conference Series: Materials Science and Engineering: 3rd National Conference on Wind & Earthquake Engineering and International Seminar on Sustainable Construction Engineering*, Kuala Lumpur, Malaysia, vol. 712, no. 1, pp. 1-7, 2020. [CrossRef] [Google Scholar] [Publisher Link]

[6] Ahmad Jabbar Hussain Alshimmeri, and Hadi Nasir Ghadhban Al-Maliki, “Structural Behavior of Reinforced Concrete Hollow Beams under Partial Uniformly Distributed Load,” *Journal of Engineering*, vol. 20, no. 7, pp. 130-145, 2014. [CrossRef] [Google Scholar] [Publisher Link]

[7] Ahmed Ismail el-kassas, Hassan Mohammed Hassan, and Mohammed Abd El Salam Arab, “Effect of Longitudinal Opening on the Structural Behavior of Reinforced High-strength Self-Compacted Concrete Deep Beams,” *Case Studies in Construction Materials*, vol. 12, pp. 1-10, 2020. [CrossRef] [Google Scholar] [Publisher Link]

[8] Ahmmad A. Abbass et al., “Flexural Response of Hollow High Strength Concrete Beams Considering Different Size Reductions,” *Structures*, vol. 23, pp. 69-86, 2020. [CrossRef] [Google Scholar] [Publisher Link]

[9] A.S. Elamary, I.A. Sharaky, and M. Alqurashi, “Flexural Behaviour of Hollow Concrete Beams under Three Points Loading: Experimental and Numerical Study,” *Structures*, vol. 32, pp. 1543-1552, 2021. [CrossRef] [Google Scholar] [Publisher Link]

[10] S. Manikandan, S. Dharmar, and S. Robertravi, “Experimental Study on Flexural Behaviour of Reinforced Concrete Hollow Core Sandwich Beams,” *International Journal of Advance Research in Science and Engineering*, vol. 4, no. 1, pp. 937-946, 2015. [Google Scholar]

[11] Nibin Varghese, and Anup Joy, “Flexural Behaviour of Reinforced Concrete Beam with Hollow Core at Various Depth,” *International Journal of Science and Research*, vol. 5, no. 5, pp. 741-746, 2016. [Google Scholar] [Publisher Link]

[12] IIbrahim A. Sharaky, Ahmed S. Elamary, and Yasir M. Alharthi, “Flexural Response and Failure Analysis of Solid and Hollow Core Concrete Beams with Additional Opening at Different Locations,” *Materials*, vol. 14, no. 23, pp. 1-27, 2021. [CrossRef] [Google Scholar] [Publisher Link]

[13] Arun Murugesan, and Arunachalam Narayanan, “Influence of a Longitudinal Circular Hole on Flexural Strength of Reinforced Concrete Beams,” *Practice Periodical on Structural Design and Construction*, vol. 22, no. 2, 2016. [CrossRef] [Google Scholar] [Publisher Link]

[14] Arun Murugesan, and Arunachalam Narayanan, “Deflection of Reinforced Concrete Beams with Longitudinal Circular Hole,” *Practice Periodical on Structural Design and Construction*, vol. 23, no. 1, pp. 1-15, 2017. [CrossRef] [Google Scholar] [Publisher Link]

[15] Fahad M. Alharthi et al., “Flexural Behavior of Concrete Hollow-Core Beams Reinforced with GFRP Bars: Experimental and Analytical Investigation,” *Arabian Journal for Science and Engineering*, vol. 49, no. 4, pp. 5267-5286, 2023. [CrossRef] [Google Scholar] [Publisher Link]

[16] Bassam Qasim Abdulrahman, “Flexural Behaviour of Hollow Reinforced Concrete Continuous Beams Reinforced with GFRP Bars,” *Discover Civil Engineering*, vol. 2, no. 1, pp. 1-20, 2025. [CrossRef] [Google Scholar] [Publisher Link]

[17] Walid Mansour et al., “Behavior of Hollow Self-Compacted Concrete Beams Reinforced with Aluminum Sections,” *Structures*, vol. 52, pp. 549-567, 2023. [CrossRef] [Google Scholar] [Publisher Link]

[18] Wenping Du et al., “Experimental Investigation of Predamaged Hollow Core Beams Shear-Strengthened with ESS–HCC,” *Structures*, vol. 61, pp. 1-14, 2024. [CrossRef] [Google Scholar] [Publisher Link]

[19] Wenping Du et al., “Investigating the Shear Behaviors of Hollow Core Beams Strengthened with ESS-HCC and Shear Steel Rebars,” *Advances in Structural Engineering*, vol. 28, no. 6, pp. 1058-1074, 2025. [CrossRef] [Google Scholar] [Publisher Link]

[20] Jing Yang et al., “Experimental Investigation and Evaluation of Shear Performance of Hollow Slab Beams Strengthened by Cavity Grouting Method,” *Case Studies in Construction Materials*, vol. 20, pp. 1-19, 2024. [CrossRef] [Google Scholar] [Publisher Link]

[21] “*318-19(22): Building Code Requirements for Structural Concrete and Commentary (Reapproved 2022)*,” American Concrete Institute, pp. 1-624, 2022. [Google Scholar] [Publisher Link]

[22] *BS EN 933-1:2012 Tests for Geometrical Properties of Aggregates - Determination of Particle Size Distribution. Sieving Method*, BSI, 2012. [Publisher Link]

[23] A F Ahmad et al., "Influence of Polymer Coated Aggregate on the Aggregate Impact and Crushing Value," *IOP Conference Series: Materials Science and Engineering: The International Postgraduate Conference on Mechanical Engineering*, Pekan, Malaysia, vol. 1078, pp. 1-11, 2021. [CrossRef] [Google Scholar] [Publisher Link]

[24] *ASTM C496/C496M-17 Standard Test Method for Splitting Tensile Strength of Cylindrical Concrete Specimens*, ASTM International, 2026. [Google Scholar] [Publisher Link]

[25] Ahmed M. Diab et al., "Bond Behavior and Assessment of Design Ultimate Bond Stress of Normal and High Strength Concrete," *Alexandria Engineering Journal*, vol. 53, no. 2, pp. 355-371, 2014. [CrossRef] [Google Scholar] [Publisher Link]

[26] Robert Park, "Evaluation of Ductility of Structures and Structural Assemblages from Laboratory Testing," *Bulletin of the New Zealand Society for Earthquake Engineering*, vol. 22, no. 3, pp. 155-166, 1989. [CrossRef] [Google Scholar] [Publisher Link]

[27] Baiq Asiani, Rudy Djamaluddin, and Fakhruddin, "The Effect of Bar Ductility Reinforcement on the Flexural Behavior of Reinforced Concrete Beams," *Engineering, Technology & Applied Science Research*, vol. 16, no. 2, pp. 34431-34436, 2026. [CrossRef] [Google Scholar] [Publisher Link]

[28] Charles S. Whitney, "Plastic Theory of Reinforced Concrete Design," *Transactions of the American Society of Civil Engineers*, vol. 107, no.1, 1942. [CrossRef] [Google Scholar] [Publisher Link]